Applied Microbiology and Biotechnology (2024) 108:75
https://doi.org/10.1007/s00253-023-12877-7

GENOMICS, TRANSCRIPTOMICS, PROTEOMICS

# Adaptive laboratory evolution for improved tolerance of vitamin K in *Bacillus subtilis*

**Xiumin Ding[1,2,3] · Zhiming Zheng[1] · Genhai Zhao[1] · Li Wang[1] · Han Wang[1] · Peng Wang[1]**

Received: 19 June 2023 / Revised: 10 October 2023 / Accepted: 30 October 2023


## Abstract

Menaquinone-7 (MK-7), a subtype of vitamin $K_2$ ($VK_2$), assumes crucial roles in coagulation function, calcium homeostasis, and respiratory chain transmission. The production of MK-7 via microbial fermentation boasts mild technological conditions and high biocompatibility. Nevertheless, the redox activity of MK-7 imposes constraints on its excessive accumulation in microorganisms. To address this predicament, an adaptive laboratory evolution (ALE) protocol was implemented in *Bacillus subtilis* BS011, utilizing vitamin $K_3$ ($VK_3$) as a structural analog of MK-7. The resulting strain, BS012, exhibited heightened tolerance to high $VK_3$ concentrations and demonstrated substantial enhancements in biofilm formation and total antioxidant capacity (T-AOC) when compared to BS011. Furthermore, MK-7 production in BS012 exceeded that of BS011 by 76% and 22% under static and shaking cultivation conditions, respectively. The molecular basis underlying the superior performance of BS012 was elucidated through genome and transcriptome analyses, encompassing observations of alterations in cell morphology, variations in central carbon and nitrogen metabolism, spore formation, and antioxidant systems. In summation, ALE technology can notably enhance the tolerance of *B. subtilis* to VK and increase MK-7 production, thus offering a theoretical framework for the microbial fermentation production of other $VK_2$ subtypes. Additionally, the evolved strain BS012 can be developed for integration into probiotic formulations within the food industry to maintain intestinal flora homeostasis, mitigate osteoporosis risk, and reduce the incidence of cardiovascular disease.

### Key points

- *Bacillus subtilis was evolved for improved vitamin K tolerance and menaquinone-7 (MK-7) production*
- *Evolved strains formed wrinkled biofilms and elongated almost twofold in length*
- *Evolved strains induced sporulation to improve tolerance when carbon was limited*

**Keywords** *Bacillus subtilis* · Adaptive laboratory evolution · Vitamin K · Genome resequencing · Transcriptome analysis

## Introduction

Vitamin K (VK), a fat-soluble micronutrient, is characterized structurally by the presence of a 2-methyl-1,4-naphthoquinone ring and varying numbers of isoprene residues linked to the C-3 position of the ring (Ren et al. 2020). VK can be categorized into vitamin $K_1$ (phylloquinone, $VK_1$), vitamin $K_2$ (menaquinone-n, MK-n, $VK_2$), and vitamin $K_3$ (menadione, $VK_3$). These compounds are structural analogs, with $VK_3$ being a synthetic compound devoid of a side chain and $VK_2$ comprising native compounds featuring variable side chains consisting of 4–13 isoprene units. In terms of physiological function, $VK_2$ plays a pivotal role in enhancing coagulation and mitigating osteoporosis, making them widely utilized as dietary supplements or pharmaceutical agents in the food and pharmaceutical industries (Chen et al. 2020; Liao et al. 2021; Ren et al. 2020). Among the $VK_2$ subtypes, menaquinone-7 (MK-7) stands out as it can be directly absorbed and utilized by the human body, boasting a longer half-life than other $VK_2$ forms (Chen et al. 2020).

✉ Zhiming Zheng
zhengzhiming2014@163.com

✉ Peng Wang
pengwang@ipp.ac.cn

1 Institute of Intelligent Machines, Hefei Institutes of Physical Science, Chinese Academy of Sciences, Hefei, China

2 Department of Health Inspection and Quarantine, Wannan Medical College, Wuhu, China

3 University of Science and Technology of China, Hefei, China

Published online: 09 January 2024

*Bacillus subtilis* (*B. subtilis*) exhibits the capacity to produce a diverse range of $VK_2$ isoforms, with MK-7 accounting for over 90% of the total output (Liao et al. 2021). MK-7 functions as a coenzyme in the respiratory chain, and its intracellular accumulation is relatively low, with 20–60% of MK-7 being secreted into the broth during fermentation (Ren et al. 2020). This phenomenon may partly stem from the potential toxicity of quinones, such as ubiquinone and menaquinone, which can act as oxidants, electrophiles, or both (Fritsch et al. 2019; Liao et al. 2021). *B. subtilis* is favored as a cell factory due to its highly efficient protein secretion system and adaptable metabolism (Su et al. 2020). Additionally, *B. subtilis* demonstrates notable resistance to environmental stresses like high pH, temperature, and the presence of organic solvents (Park et al. 2021), rendering it an ideal candidate for MK-7 production. Despite significant progress in enhancing MK-7 synthesis through strategies like strain modification to augment biosynthesis capacity (Cui et al. 2019; Yang et al. 2019), process optimization to improve synthesis efficiency (Berenjian et al. 2014; Wang et al. 2019), and innovative bioreactor design to expedite industrialization (Ren et al. 2020), high MK-7 concentrations can substantially impede host cell growth, leading to detrimental changes culminating in cell lysis (Cui et al. 2019). To date, the biosynthesis of MK-7 still falls short of meeting industrial requirements. Thus, enhancing the tolerance of chassis cells to VK may represent a breakthrough for MK-7 synthesis.

Adaptive laboratory evolution (ALE) has emerged as an innovative approach for generating evolved microbial strains with desired characteristics, enabling microorganisms to rapidly adapt to changing environments (Dorau et al. 2021; Mavrommati et al. 2021; Sun et al. 2018b). In contrast to directly modifying specific enzymes and employing rational engineering strategies, ALE can yield non-intuitive beneficial mutations within various regulatory gene regions, thereby avoiding issues such as reduced cell adaptation associated with gene editing technologies (Sun et al. 2018b). Advances in laboratory automation and sequencing technologies have laid the groundwork for the widespread adoption of ALE (Dorau et al. 2021). ALE, when combined with high salinity, has been employed to enhance antioxidant systems and lipid accumulation, resulting in the final strain ALE150 displaying an overall increase in total antioxidant capacity (T-AOC) and lipid yield compared to the initial strain (Sun et al. 2018a). ALE has also been effectively utilized to optimize the lipid accumulation capabilities of *Yarrowia lipolytica* (Daskalaki et al. 2019). Furthermore, ALE has proven successful in enhancing *Saccharomyces cerevisiae*'s tolerance to ethanol, thereby improving the fermentation ability and ethanol yield of the evolved strains (Mavrommati et al. 2023).

In the present study, *B. subtilis* BS011, a MK-7-producing strain, underwent ALE to yield BS012, which exhibited robust tolerance to high $VK_3$ concentrations. Subsequently, we evaluated the impact of oxidative toxicity on the performance of BS012 by characterizing cell morphology, antioxidant systems, and fermentation properties. Moreover, we gained a deeper understanding of the mechanisms underlying BS012's tolerance to high $VK_3$ concentrations during extended ALE through comparative genomic and transcriptomic analyses. This work contributes to enhancing the adaptability of strain BS012 to $VK_3$ and its capacity to synthesize MK-7, thus addressing the requirements of the food industry.

## Materials and methods

### Microorganism and culture conditions

*B. subtilis* BS011 (accession number: CCTCC AB 2023167) was used as the starting strain. All strains were cultivated in Luria–Bertani (LB) medium or agar plates at 37 °C. The fermentation medium for the shake flasks was composed of 30 mL/L glycerol, 60 g/L soy peptone, 5 g/L yeast extract, 3 g/L $K_2HPO_4$, and 0.5 g/L $MgSO_4.7H_2O$, with a pH of 7.3.

### ALE experiments

To determine the minimum inhibitory concentration of $VK_3$ against *B. subtilis*, the seed culture was inoculated into shake flasks containing 50 mL of fermentation medium, and $VK_3$ was added to obtain final concentrations of 0, 2.0, 4.0, 6.0, 8.0, and 10.0 mg/L. After incubation in 37 °C shaker (220 r/m) for 24 h, the $OD_{600}$ value of the culture was measured.

ALE was performed using serial passaging. Seed culture (1.5% inoculation scale) was inoculated into fermentation medium supplemented with 6.0 mg/L $VK_3$ and cultivated in a shaker at 37 °C and 220 r/m for 24 h. During the ALE process, the $VK_3$ concentration was gradually increased from 6.0 to 60.0 mg/L, with an increment of 3.0 mg/L in each step. The strains were cultivated twice (24 h per propagation cycle) for each concentration. Finally, the strains able to tolerate 60.0 mg/L of $VK_3$ were cultured for 24 h three times under 60.0 mg/L to obtain a genetically stable generation. To isolate evolved mutants, cultures were struck onto LB media plates containing 60.0 mg/L $VK_3$. The largest colony was selected and named BS012 (accession number: CCTCC M 20232563).

### Shake-flask fermentation of the engineered *B. subtilis*

Shake-flask fermentation was performed in triplicate, according to the method described by Cui (Cui et al. 2019). Strains were inoculated into the seed culture and cultivated

in a shaker at 37 °C and 220 r/m for 12 h. Next, 5 mL of seed culture was inoculated into 50/500 mL fresh fermentation medium and cultured at 40 °C and 220 r/m for 120 h. One milliliter of fermentation medium was sampled, and the cell density was measured at 600 nm.

## Determination of T-AOC

The T-AOC of the cells was determined using a BC1315 kit (Solarbio, Beijing, China) according to the manufacturer's instructions. Cells in the stationary phase (~60 h) were collected, washed with ice-cold phosphate-buffered saline (PBS), immediately frozen in liquid nitrogen, and pretreated using a homogenizer. The ice-cold extract was then centrifuged at 8000 × *g* for 8 min at 4 °C, and the supernatants were used for T-AOC measurements. The total protein concentration was measured using an Enhanced BCA Protein Assay Kit (Beyotime, Shanghai, China). The total protein content of crude enzyme was calculated using the following empirical calibration equation:

$$\text{Protein content} = 0.5489 \times \text{OD}_{562} + 0.0435 \quad (1)$$

## Determination of biofilm andNADH/NAD$^+$ instatic culture of *B. subtilis*

Seed cultures of BS011 and BS012 (inoculation scale of 10.0%) were introduced into 12-well plates containing 4 mL fermentation medium and cultured at 37 °C for 3 days. Biofilms were harvested, lyophilized, and weighed. NADH/NAD$^+$ levels in *B. subtilis* were quantified using a commercially available kit (Solarbio, Beijing, China) according to the manufacturer's instructions. $\text{NAD}_{\text{total}}$ (NAD$^+$ and NADH) or NADH levels were measured via a colorimetric assay at 450 nm utilizing a SpectraMax i3x (Molecular Devices, USA). The NADH/NAD$^+$ ratio was calculated as follows:

$$\text{NADH/NAD}^+ = \text{NADH}/(\text{NAD}_{\text{total}} - \text{NADH}) \quad (2)$$

## MK-7 extraction and analysis

MK-7 was extracted from the biofilm and fermentation medium following our previous study (Ding et al. 2022). Briefly, 1 mL of fermentation broth was centrifuged at 8000 × *g* for 6 min, and 2 mL of an n-hexane and isopropanol mixture (v/v, 2:1) was added to the supernatant. After shaking for 2 h, 1 mL of n-butanol was introduced. The mixture underwent an additional 1-h shaking period and was subsequently centrifuged at 6000 × *g* for 5 min to separate the two phases. The organic phases were collected to recover the extracted MK-7. Simultaneously, cell precipitates or biofilms were oven-dried and dissolved in 2 mL of ethanol. After shaking for 2 h and centrifugation at 9000 × *g* for 10 min, the organic phases were collected and filtered to obtain an extract containing intracellular MK-7.

Finally, the concentration of MK-7 in the organic phase was determined via high-performance liquid chromatography (Shimadzu, Japan) using a UV detector and VP-ODS C18 column (5 μm, 150 mm × 4.6 mm, Shimadzu, Japan). The mobile phase consisted of a methanol and dichloromethane mixture (v/v, 4:1); the flow rate was set at 1 mL/min, and the oven temperature was maintained at 35 °C. A wavelength of 254 nm was employed for calibration and analysis. The MK-7 calibration curve demonstrated linearity within the range of 10 to 150 mg/L ($R^2 = 0.999$).

## Bacterial morphological observation

Sample preparation for scanning electron microscopy (SEM) adhered to the method described by Fang et al. (Fang et al. 2019). In brief, cells in the stationary phase (approximately 60 h) were pelleted, washed with PBS, and fixed with 2.5% glutaraldehyde for 2–4 h at 4 °C. Dehydration was accomplished using a series of ethanol solutions (10, 30, 50, 70, 80, 90, and 100%), and the samples were subsequently air-dried at room temperature (25 °C). Following these steps, the samples were sputter-coated with platinum and examined using a GeminiSEM 500 scanning electron microscope (Schottky field emission scanning electron microscope, Hitachi High-Tech Corporation, California, USA).

## Membrane potential (ΔΨ) detection

The determination of ΔΨ followed a previously described protocol (Rao et al. 2007). Cells in the stationary phase (approximately 60 h) were collected from the fermentation medium, diluted to $1 \times 10^9$ cfu/mL with PBS, and stained with 10 μL of 3 mM fluorescent dye—3,3-diethyloxa-carbocyanine iodine (DiOC2(3)) for 30 min at 37 °C. After staining, the cells were harvested by centrifugation at 8000 × *g* for 8 min and resuspended in PBS. The stained cells were analyzed by fluorescence-activated cell sorting using 488 nm excitation and emission filters suitable for fluorescein and Texas Red dye. ΔΨ was calculated as the ratio of red-to-green fluorescence.

## Genome resequencing and transcriptome analysis

Evolved strain BS012 and the initial strain BS011, both in the stationary phase (approximately 60 h), were harvested from shake-flask cultures and promptly frozen in liquid nitrogen. Genome resequencing and analysis were conducted by OE Biotech Co., Ltd. (Shanghai, China). RNA extraction, library construction, transcriptome sequencing, and

global gene analysis were performed by GENE DENOVOS (Guangzhou, China).

## Results

### Screening of promising MK-7-producing strains using ALE

Prior investigations have traditionally utilized biomass and/or production as benchmarks for assessing the performance of MK-7-producing strains. In a recent study, we redesigned central carbon pathways and enhanced the compatibility between material and energy metabolism within MK-7 synthesis pathways in *B. subtilis* 168. This endeavor culminated in the creation of a recombinant strain, BS011, capable of yielding 53.07 mg/L of MK-7 in shaker flasks (Ding et al. 2022). Nonetheless, strains demonstrating superior performance should not only exhibit high MK-7 productivity but also possess robust antioxidant defenses against MK-7 oxidation. In this study, we further investigated the impact of enhanced chassis cell tolerance on MK-7 synthesis in the engineered strain BS011. As $VK_3$, a structural analog of MK-7, shares oxidation properties akin to those of MK-7 but is more cost-effective, we opted to employ $VK_3$-induced stress for ALE in *B. subtilis* BS011. BS011 experienced pronounced growth inhibition at 8.0 mg/L $VK_3$ and mild inhibition at 6.0 mg/L $VK_3$, resulting in an $OD_{600}$ value of approximately 2.187 (Figure S1). This phenomenon may be attributed to the activation of stress responses, necessitating the reallocation of cellular resources, thereby impeding growth potential. Consequently, we selected 6.0 mg/L as the initial ALE concentration. Following 45 generations of evolution, the tolerance of BS011 to $VK_3$ increased from 6.0 to 60.0 mg/L (Fig. 1a). The largest clone from the evolved population, designated as BS012, was isolated, effectively restoring the final cell density and growth rate to levels comparable to those of BS011 in the fermentation medium (Fig. 1b). These results underscore the efficacy of employing ALE to enhance host tolerance to products, thereby overcoming growth inhibition—an approach characterized by its simplicity and effectiveness.

### Effects of ALE on cell states and MK-7 production of strains in static culture

*B. subtilis* exhibits the capability to form diverse types of biofilms, including intricate surface colonies on agar plates and floating biofilms, known as pellicles, at the air-to-liquid interface (Hobley et al. 2015). Biofilms represent a congregation of closely associated bacteria enveloped by a self-generated extracellular matrix that establishes conditions conducive to survival in challenging environments (Fulaz et al. 2019). When cultivated on agarose plates, BS011 displayed colony morphology characterized by a dirty white appearance, irregular edges, and a rough surface (Fig. 2a, b). In contrast, BS012 exhibited markedly more wrinkled and drier morphology (Fig. 2c, d). Investigation into pellicle formation at the air-to-liquid interface revealed that BS012 cells predominantly congregated on the medium's surface, forming multiple wrinkled biofilms (Fig. 2f), while BS011 cells were primarily located at the medium's bottom, forming only a few biofilms (Fig. 2e). After 72 h of incubation in 12-well plates, the biofilm biomass in BS011 and BS012 reached 4.17 and 11.29 g/L, respectively (Fig. 2g). Moreover, from the biofilms of BS012, 1.51 μg/mg MK-7 was extracted, representing a notable 75.71% increase

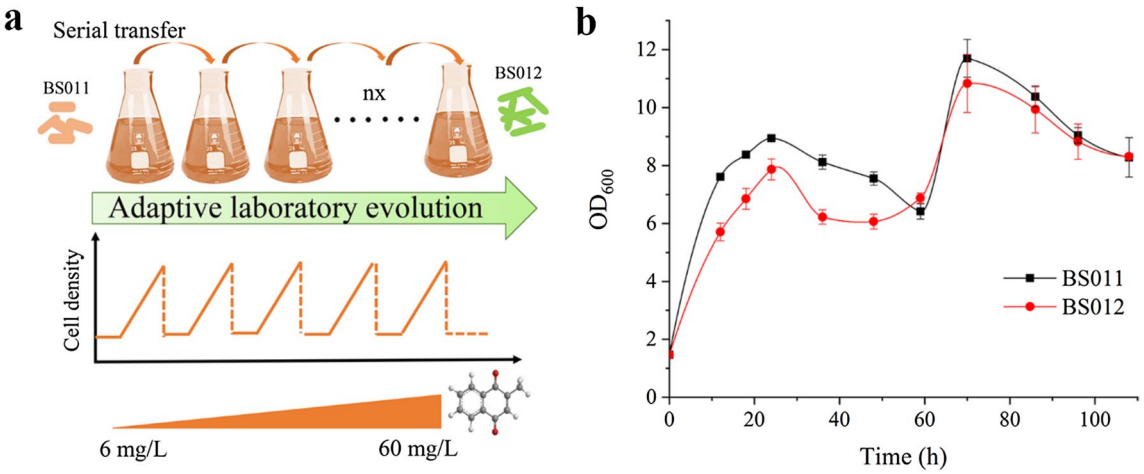


**Fig. 1** ALE to improve $VK_3$ tolerance. **a** Schematic diagram of the ALE process. Starting at 6.0 mg/L $VK_3$ in the fermentation medium, surviving cultures were inoculated into fresh media with increasing $VK_3$ concentrations, 3.0 mg/L, every round. BS012 was isolated after 45 generations of evolution. **b** Growth curves of BS011 and BS012. Squares represent the growth of BS011. Circles represent the growth of BS012. The experiments were carried out in triplicates. Error bars represent the standard deviation from the mean

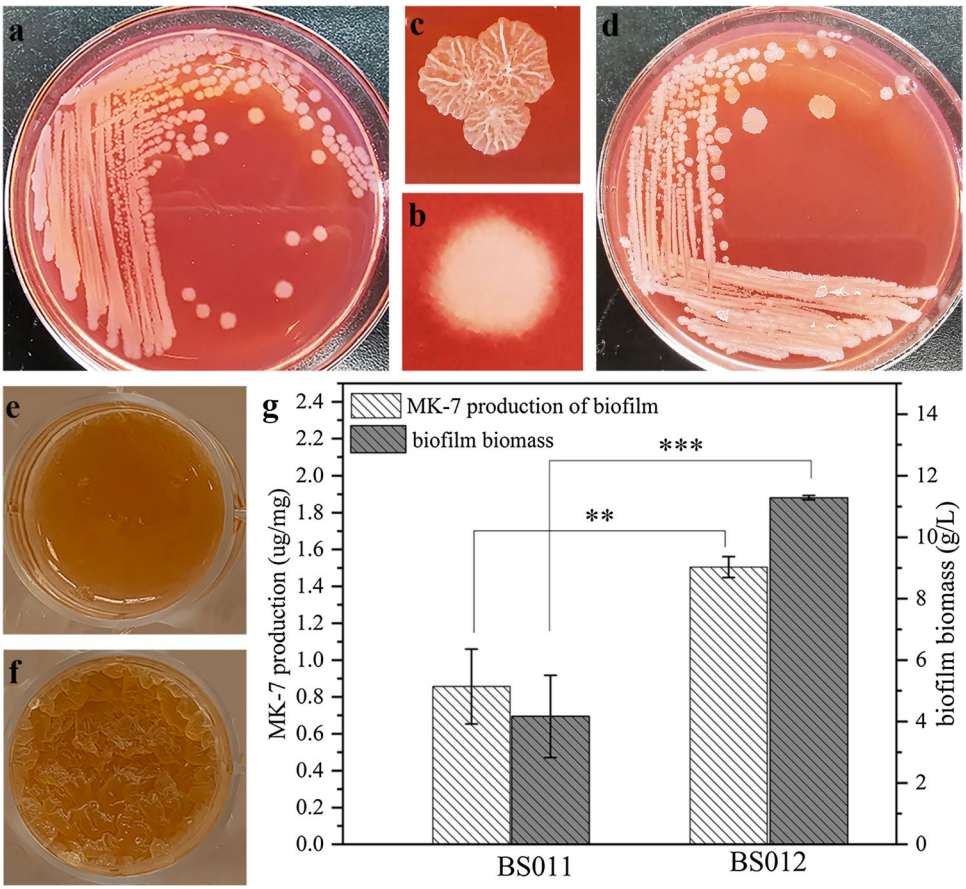


**Fig. 2** ALE effects on morphological and MK-7 production of strains in static culture **a** and **d** show the colony morphology of BS011 and BS012 on the plate with carmine. **b** and **c** are the partial enlarged images of **a** and **d**, respectively. **e** and **f** represent pellicle biofilm formation in 12-well plate cultures of BS011 and BS012, respectively. **g** The biomass and MK-7 titers of biofilms in BS011 and BS012 after 72 h incubation in 12-well plates. Results are presented as the mean of three replicates, and error bars represent the standard deviation (SD). Statistical difference was determined using a one-tailed Student's *t*-test. $^{**}p \leq 0.01$ and $^{***}p \leq 0.001$

compared to BS011 (Fig. 2g). To assess the cellular redox state, we examined the ratio of NADH/$NAD^+$. The results, presented in Figure S2, indicate that the NADH/$NAD^+$ ratio in BS012 (1.64) reflects a higher level of reduction compared to the NADH/$NAD^+$ ratio in BS011 (0.88). These findings underscore that subjecting *B. subtilis* to ALE with high $VK_3$ stress facilitated the production of multiple wrinkled biofilms and efficient MK-7 synthesis in static culture.

## Effects of ALE on morphology and MK-7 production of strains in shake culture

SEM analysis revealed that BS012 cells (Fig. 3b, d) exhibited a nearly two-fold increase in length compared to BS011 cells (Fig. 3a, c). Flow cytometry measurements indicated higher forward and side scattering values for BS012 in comparison to those for BS011 (Fig. 3e). Side scattering (SSC) reflects the refractivity of the cell cytoplasm and nuclear membrane, while forward scattering (FSC) is closely associated with cell size. These observations further underscore that BS012 not only possesses a larger cell volume but also exhibits increased surface complexity, consistent with the SEM findings. These findings align with previous studies that demonstrated an approximately two-fold increase in cell elongation in response to butanol stress in *B. subtilis* (Gao et al. 2020; Vinayavekhin et al. 2015). After 120 h of fermentation in 500 mL flasks, the total MK-7 titer in BS012 reached 64.86 mg/L, representing a noteworthy 22.22% increase compared to BS011. Notably, the intracellular MK-7 content in BS012 accounted for 68.77% of the total MK-7 content in the fermentation medium, whereas in BS011, it accounted for only 42.80% of the total amount (Fig. 3f). This suggests that BS011 may have a limited capacity to accommodate MK-7, leading to its secretion outside the cell to alleviate oxidative stress. In contrast, BS012 predominantly produces MK-7 intracellularly, with only a small portion being secreted extracellularly. These results provide support for the notion that ALE enhances strain tolerance and increases MK-7 production in shake culture. Taken together, these observations indicate that BS012 adapts to changes in the external environment through morphological changes, a phenomenon previously described (Vinayavekhin et al. 2015).

## Effects of ALE on the intracellular redox system of *B. subtilis* in shake culture

Antioxidant capacity was used as a key performance indicator of the evolved strain BS012. Antioxidant systems,

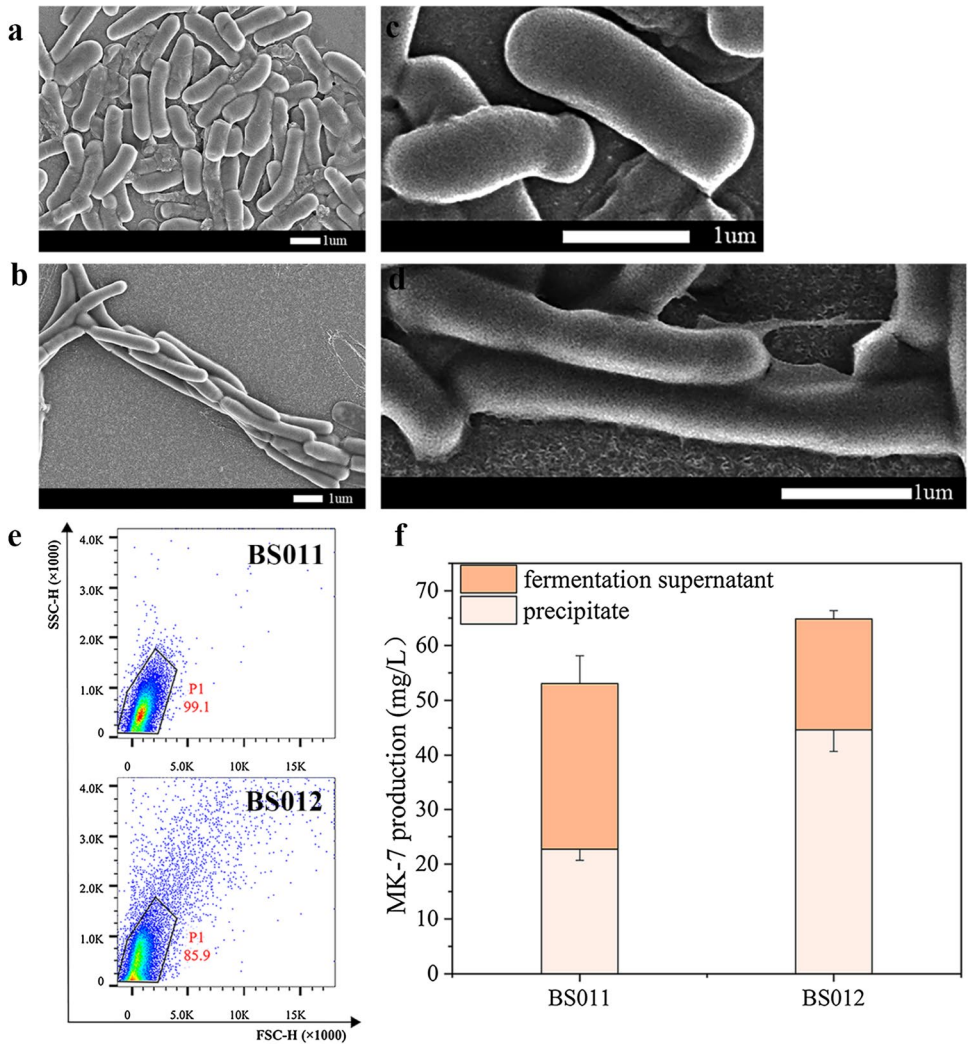


**Fig. 3** ALE effects on morphological and MK-7 production of strains in shake culture **a** and **b** represent SEM diagram of BS011and BS012. **c** and **d** are partial enlarged diagrams of **a** and **b** (magnification of × 80,000), respectively. **e** SSC versus FSC scatter diagram of BS011and BS012. Population 1 (P1) represents the proportion of cells. **f** MK-7 production of fermentation supernatants and precipitate in BS011 and BS012 after 120 h fermentation in 500 mL flasks. Results are presented as the mean of three replicates and error bars represent the standard deviation (SD)

which comprise enzymatic and non-enzymatic systems, play vital roles in counteracting various types of oxidative stress. The effect of ALE with high $VK_3$ concentrations on *B. subtilis* was investigated by the overall T-AOCs of BS011 and BS012, measured during the stationary phase (~ 60 h). Experimental results showed that the T-AOC value of BS012 was 6.51-fold higher than that of BS011, reaching 1.65 U/mg (Fig. 4a). Long-term ALE at high $VK_3$ concentrations is an effective approach for improving the antioxidant capacity of *B. subtilis*. To further explore the effect of our ALE approach on cellular physiological functions, the ΔΨ, a component of the proton motive force involved in ATP generation, was evaluated using the potential-sensitive probe DiOC2(3) (Arjes et al. 2020). Approximately 20,000 cells were collected for the assay, and the red/green mean fluorescence intensity ratio was positively correlated with ΔΨ. As shown in Fig. 4b, carbonyl cyanide 3-chlorophenylhydrazone-treated cells (positive control) with a fully depolarized ΔΨ displayed a low red/green ratio of 0.9075, whereas BS011 cells (negative control) showed a normal membrane potential, with a red/green ratio of 1.2619. The red/green ratio of BS012 was 1.2712, which was not significantly different from that of BS011. These results demonstrated that physiological functions in BS012 were not affected, although ALE promoted a larger cell morphology.

## Genome resequencing and analysis of evolved strains

The evolved strain BS012 and the original strain BS011 were re-sequenced using the Illumina HiSeq X Ten platform and aligned with the *B. subtilis* 168 reference genome (PRJNA626600). In contrast to BS011, nonsynonymous SNVs in BS012 include aspartate kinase III (ThrD), which catalyzes the synthesis of aspartate 4-phosphate, exists within a variable network that supports the synthesis of nine amino acids and several other metabolites, such as bacterial sporulation, methylation reaction, and cell wall crosslinking (Manjasetty et al. 2014); molybdopterin synthase (MoaD), involved in anaerobic nitrate respiration;

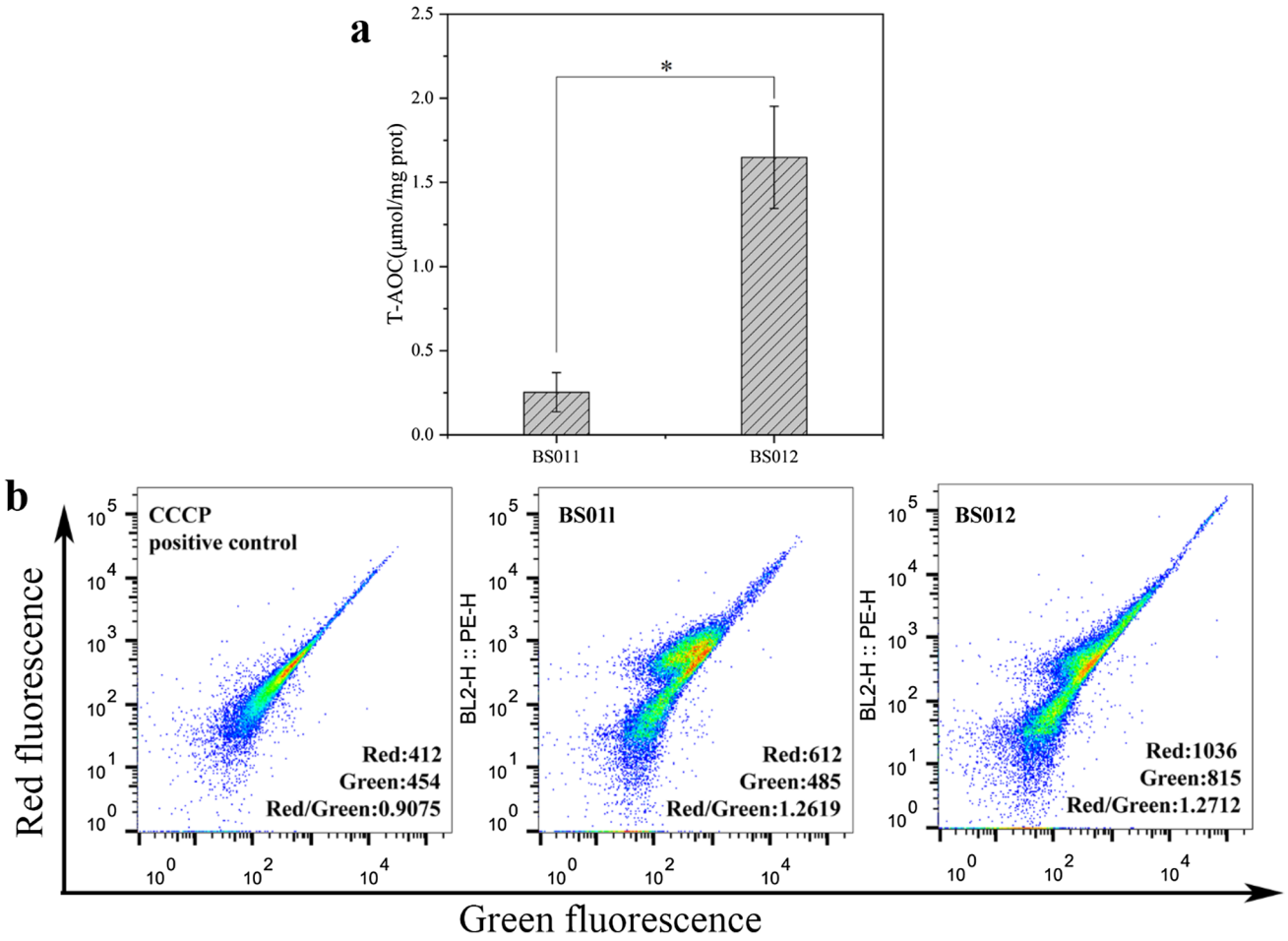


**Fig. 4** ALE effects on the physiological function of *B. subtilis* in shake culture. **a** T-AOC and **b** the ΔΨ of BS011 and BS012 was measured after 60 h fermentation in 500 mL flasks. Red/green mean fluorescence intensity ratio is positively correlated with ΔΨ. Results are presented as the mean of three replicates, and error bars represent the standard deviation (SD). Statistical difference was determined using a one-tailed Student's *t*-test. $^{*}p \leq 0.05$

UDP-N-acetylglucosamine 4,6-dehydratase (EpsC) and protein tyrosine kinase (EpsB), related to biofilm formation; two-component sensor kinase (WalK), which coordinates cell wall remodeling and cell division by controlling the transcription of autolysin and its repressor genes. In addition, the transcriptional regulator (SinR), which controls biofilm formation, has a bp frameshift Indel. We also found a C → A alteration in the upstream of *dhbF*, related to the biosynthesis of siderophore in BS012 (Table S1). In addition, the genome-wide coverage distribution map of the samples showed that large fragments in BS012 may be missing during ALE (Figure S3). Overall, genome resequencing analysis showed that evolved strain BS012 was genetically mutated at the genetic level, associated with central nitrogen metabolism, anaerobic nitrate respiration, biofilm formation, cell morphology changes, and attenuation of oxidative stress.

## Comparative transcriptome analysis of *B. subtilis* in shake culture

Transcriptomic data were analyzed to elucidate the mechanisms involved in the changes in cell morphology and improved tolerance of the evolved strain BS012 during ALE. We found 730 differentially expressed genes (DEGs) in BS012 compared with those in BS011, comprising 193 upregulated and 537 downregulated genes (Fig. 5a). Of which, some of DEGs based on significant value were sorted into regulons, and subsets of the most significantly changed regulons are displayed in Voronoi transcriptome treemaps (Fig. 5b). The FapR, SigM, and SigV regulons were related to cell morphology; Fur and CcpA regulons were associated with iron, sulfur, and central carbon metabolism; Fnr, Cody, NrdR, ThrA, and ArgR regulons were related to anaerobic respiration and central nitrogen metabolism; SigE, SpovT,

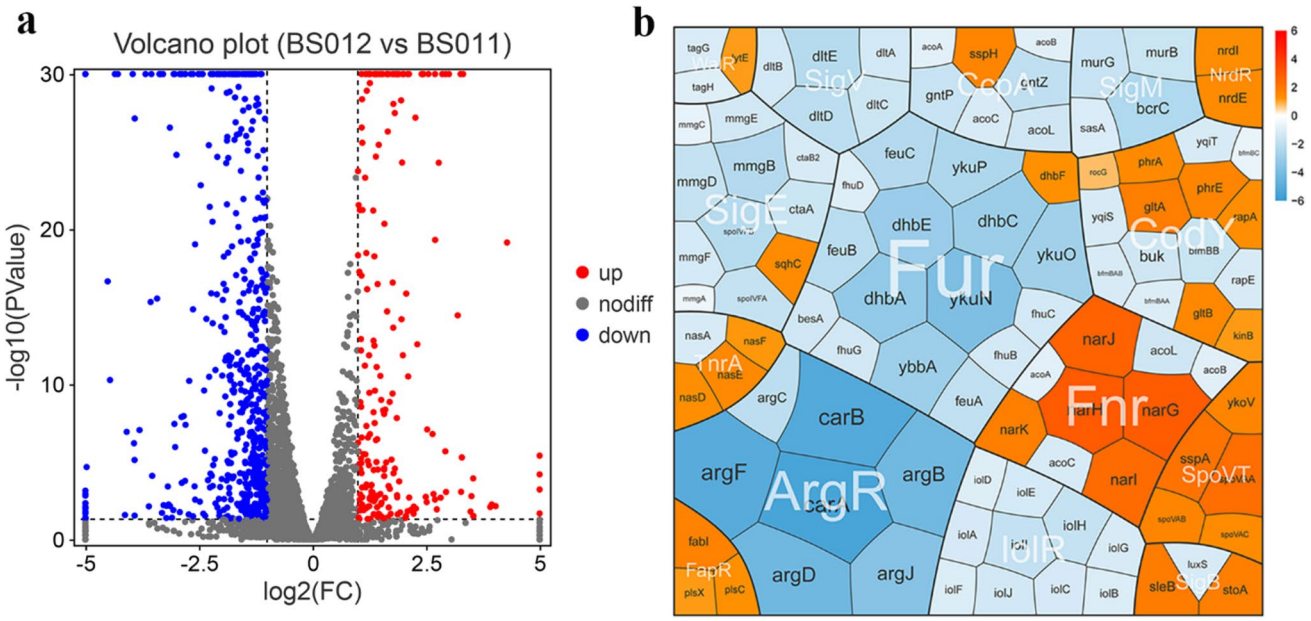


**Fig. 5** RNA-seq transcriptomics of BS012 after adaptation to $VK_3$ oxidative toxicity in shake culture. **a** Volcano plot of differential transcription levels as determined by RNA sequencing ($N=3$). **b** The transcriptome treemap of BS012 during ALE with high $VK_3$ stress showed significant changes in FapR, SigM, SigV, Fur, CcpA, Fnr, Cody, NrdR, ThrA, ArgR, SigE, SpovT, and SigB regulons. Differential gene expression of BS012 after 120 h fermentation in shake culture was shown as log2-fold changes in the transcriptome treemap. Based on the SubtiWiki database, we categorized these genes as operons and regulators. Differential gene expressions are visualized using a red–blue color code where red indicates upregulated and blue indicates downregulated of transcription. Furthermore, the transcriptome data and regulons classifications of the genes presented in the transcriptome treemap are listed in Table S2

and SigB regulons were associated with spore formation and antioxidant systems.

## Mechanistic alterations regulating cell morphology and size

Cell envelopes play vital roles in various cellular functions, including growth, cell division, interactions with the environment, and resistance to antibiotics (Bitoun et al. 2012). Fatty acids are essential components of cell membranes and are crucial for normal metabolism. In BS012, the expression level of the global transcriptional repressor FapR, responsible for regulating membrane lipid biosynthesis, exhibited a significant upregulation compared to BS011, with a log2-fold change of 1.37. Moreover, other regulators like *plsX*, *fabI*, and *plsC* also showed upregulation, with log2-fold changes ranging from 1.05 to 1.66. Additionally, the expression of acetyl-CoA carboxylase (*accB*), which converts acetyl-CoA into malonyl-CoA, increased by 1.42-fold. These changes suggest that BS012 likely enhanced the synthesis of saturated fatty acids to ensure the stability and functionality of the cell membrane, possibly reducing cell membrane fluidity to prevent $VK_3$ cellular invasion (Shen et al. 2020).

In response to nutrient limitation, *B. subtilis* orchestrates a regulatory network involving two-component systems and cell wall homeostasis by sequentially activating the extracellular cytoplasmic function (ECF) σ factors (Helmann 2016). $\sigma^M$ (*sigM*), strongly induced under conditions that impede peptidoglycan synthesis, can trigger the upregulation of core pathways related to envelope synthesis and cell division (Helmann 2016). On the other hand, $\sigma^V$ (*sigV*) is closely linked to lysozyme resistance (Helmann 2016). Transcriptome analysis revealed a downregulation of the autoregulated *sigM-yhdL-yhdK* and *sigV-rsiV-oatA* operons in BS012 compared to BS011, with log2-fold changes of 0.74 and 2.88, respectively. These changes inevitably influence genes associated with cell wall synthesis. Notably, the expression of undecaprenyl pyrophosphate phosphatase (*bcrC*), responsible for producing the carrier lipid essential for cell wall synthesis, was downregulated by 2.43-fold in BS012 compared to BS011. Additionally, the expression levels of UDP-N-acetylenolpyruvoylglucosamine reductase (*murB*) and UDP-N-acetylglucosamine-N-acetylmuramyl-(pentapeptide) pyrophosphoryl-undecaprenol N-acetylglucosamine transferase (*murG*), involved in the biosynthesis of peptidoglycan precursors, exhibited downregulation by 1.66- and 1.74-fold, respectively. Furthermore, the expression of ABC transporters responsible for teichoic acid translocation, *tagG* and *tagH*, decreased by 1.17- and 1.01-fold, respectively.

## Differences in iron, sulfur, and central carbon metabolism

Fat-soluble $VK_3$ is known to penetrate cell membranes and produce $O^{2-}$, which readily oxidizes intracellular non-redox mononuclear enzymes and $[4Fe\text{-}4S]^{+}$-containing dehydratases, leading to enzyme inactivation (Loi et al. 2015; Zuber 2009). During ALE, the iron carrier bacillin synthesis (*dhbACE*), bacillin uptake (*feuABC*), isohydroxamate iron carrier uptake (*fhuBCGD*), and flavin oxygen-reducing protein (*ykuNOP*) were significantly downregulated in BS012 (log2-fold changes of 1.04–3.91). Moreover, the iron storage protein-encoding gene (*mrgA*) was downregulated by 1.46-fold. During ALE, cells reduce intracellular iron concentrations by limiting iron metabolism, consequently reducing ROS production and avoiding ferroptosis (Zuber 2009). Iron is the most common trace element related to biological functions, such as Fe-S-cluster enzymes and heme proteins (Pinochet-Barros and Helmann 2018). We found that Fe-S-cluster biosynthesis operon *sufCDSUB* was downregulated to varying degrees, with the most significant change observed in *sufB* (log2-fold change of 1.18). Moreover, the expression levels of heme synthases encoding genes, *ctaA* and *ctaB*, were significantly downregulated (log2-fold changes of 1.63 and 1.25, respectively).

When encountering ROS in the environment, protein thiols are first oxidized to Cys sulfenic acids as unstable intermediates (R-SOH), followed by irreversible over-oxidation to Cys sulfinic ($R\text{-}SO_2H$) and sulfonic acid ($R\text{-}SO_3H$) (Loi et al. 2015). Low molecular weight (LMW) thiols play important roles as thiol cofactors for several enzymes and are crucial for maintaining the reduced state of the cytoplasm (Imber et al. 2019). They can rapidly react with R-SOH forming reversible protein disulfides or mixed disulfides, termed S-thiolations (Loi et al. 2015). Cysteine is an important LMW thiol in *B. subtilis* (Loi et al. 2015). We found that the expression of *mccB*, the gene encoding cystathionine lyase, decreased 1.91-fold in BS012, suggesting a sufficient cysteine in BS012. Consequently, small molecule cysteine played an important role in maintaining the cytoplasmic redox homeostasis in BS012 during ALE (Imber et al. 2019).

Additionally, most detected metabolites in central carbon metabolism were significantly lower in BS012 than in BS011, such as the tricarboxylic acid (TCA) cycle. Transcriptome analysis showed that pyruvate dehydrogenase (*pdhABCD*), α-ketoglutarate(AKG) dehydrogenase (*odhAB*), phosphoenolpyruvate carboxykinase (*pckA*), and 2-methylcitrate synthase (*mmgD*) were all downregulated in BS012 (log2-fold changes of 0.22–1.81). Thiamin pyrophosphate and lipoic acid are important cofactors in the pyruvate dehydrogenase complex and the alpha-ketoglutarate dehydrogenase complex. The expression levels of the *tenA-tenI-thiO-thiS-thiG-thiF-thiD* and *thiM-thiE* operons, related to thiamine biosynthesis, were downregulated in BS012 (log2-fold changes of 0.87–2.05), the expression levels of *gcvH* and *lipL*, which are related to lipoic acid binding and metastasis, were significantly decreased in BS012 compared to those in BS011 (log2-fold changes of 1.73 and 1.49, respectively). The BS012 reduction in TCA cycle flux may be related to the decline in aerobic respiration for decreasing ROS production (van der Reest et al. 2018). Additionally, the expression of the myo-inositol catabolism operon *iolABCDEFGHIJ*, which yields DHAP, acetyl-CoA, $CO_2$, and NADH molecules, was significantly downregulated in BS012. This result proves that myo-inositol contained in the yeast extract has been depleted as a secondary carbon source. Overall, during ALE, BS012 accumulated excess NADPH for the reduction of disulfides in the organism during early growth, which leads to carbon source depletion and reduced central metabolism.

## Differences in nitrogen and amino acid-related metabolism

When *B. subtilis* sense fluctuations in environmental oxygen concentrations, they shift their cellular metabolism accordingly (Nakano and Zuber 1998). During respiration, different membrane-associated dehydrogenases oxidize water-soluble substrates and reduce MK-7 to menaquinol-7. Under aerobic conditions, electrons are used to reduce oxygen to water, whereas under anaerobic conditions, nitrate respiratory growth-derived electrons are transferred to nitrate to yield nitrite (Härtig and Jahn 2012). In BS012, the expression of Fnr, a transcriptional activator of anaerobically induced genes, was slightly upregulated by 0.58-fold compared to that in BS011. The assimilatory NAD(P)H-dependent nitrite reductase-encoding genes *nasD* and *nasE*, which convert nitrite into ammonia, were increased by 1.22- and 1.43-fold, respectively. In addition, the expression of the *narGHJI* operon, which encodes respiratory nitrate reductase (Nar) and is induced by Fnr, was significantly upregulated (log2-fold changes of 2.40–3.00) (Fig. 6). In *B. subtilis*, Nar is a menaquinol-7 oxidase, and the menaquinol pool is oxidized by the cytochrome b subunit NarI. Two electrons flow via heme b from NarI to the Fe-S-cluster of NarH and finally to the cytoplasmic subunit NarG, which reduces nitrate to nitrite and generates a transmembrane electrochemical gradient (Härtig and Jahn 2012; Hederstedt 2021). These results further confirm that anaerobic nitrate respiration had been activated in BS012 at 60 h of fermentation.

The regulation of central nitrogen metabolism in *B. subtilis* is closely related to intracellular glutamate and glutamine concentrations. The glutamate–glutamine metabolic balance is catalyzed by glutamine synthetase (GS)–glutamate synthetase (GOGAT)–glutamate dehydrogenase (GDH)

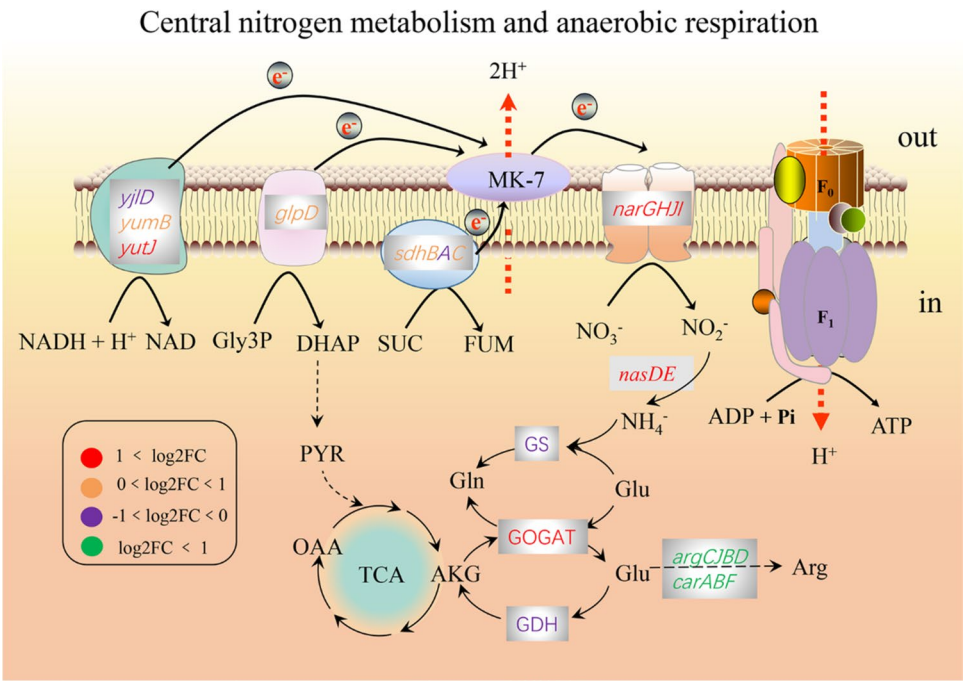


**Fig. 6** DEGs involved in anaerobic respiration and central nitrogen metabolism. The letters in the gray boxes represent the genes encoding the enzymes. Red and orange represent genes that are upregulated, while purple and green represent genes that are downregulated

systems. Compared with BS011, the expression levels of *gltA* and *gltB* (GOGAT-coding genes) were upregulated in BS012 (log2-fold changes of 1.79 and 1.46, respectively). *gudB* (GDH-coding gene) and *glnA* (GS-encoding gene) were slightly downregulated (log2-fold changes of 0.25 and 0.52, respectively). Additionally, glutaminases (*glsA*) catalyze the hydrolytic deamidation of glutamine to glutamate and $NH_4^+$, and the expression of *glsA* was downregulated by 3.81-fold. Arginine synthesis (*argC-argJ-argB-argD-carA-carB-argF*) operon was also significantly downregulated in BS012. This indicates that intracellular arginine synthesis was decreased. Evolutionary strain BS012 downregulates the expression of genes related to arginine synthesis and upregulates the expression of GOGAT to convert more glutamate to AKG, thus providing a carbon skeleton for cell growth (Commichau et al. 2006). Additionally, branched-chain α-keto acid dehydrogenase (*lpdV-bkdAA-bkdAB-bkdB*) was also significantly downregulated in BS012, which suggests that the cell reduces the waste of cellular resources by decreasing the synthesis of other amino acids.

## Spore formation and antioxidant systems

*B. subtilis* can activate different stress-response mechanisms, including general stress pathways, stringent responses, or sporulation activation (Luche et al. 2016). Through comparative transcriptome analysis, spore formation genes were upregulated in BS012 compared to the starting strain BS011 at 60 h of shake-flask culture, mainly in the following ways: quorum-sensing signaling molecules PhrA and PhrE were upregulated (log2-fold changes of 1.40 and 1.60, respectively); the regulated phosphatase RapE was significantly downregulated (log2-fold changes of 1.24); two-component sensor kinase KinB, a trigger for *B. subtilis* sporulation, was upregulated (log2-fold changes of 1.05); the expression levels of *spoVAA* and *spoVAc*, which are regulated by transcriptional regulator SpoVT, were upregulated (log2-fold changes of 2.31 and 1.35, respectively); the ABC transporter analog YtlA, expressed in mother cells, was upregulated by 11.45-fold; a spore cortex-lytic enzyme SleB, degrading the specialized cortex peptidoglycan surrounding the spore, was upregulated (log2-fold changes of 1.86); the expression of spore-specific thiol-disulfide oxidoreductase-encoding gene *stoA* was upregulated by 1.76-fold.

The mechanisms for alleviating oxidative stress and for repairing macromolecular damage are also specific for each cell type in *B. subtilis* (Zuber 2009). Spores, consisting of spore coat, membrane, and cortex, can block the entry of oxidants and are resistant to them (Zuber 2009). In addition, squalene cyclase (*sqhC*) increases the permeability of the spore membrane by synthesizing polycyclic terpenoids, thereby resisting oxidative attack. In BS012, *sqhC* expression was increased by 1.36-fold. The α/β-type small acid-soluble spore protein, encoded by *sspA*, protects spore core DNA, and its expression was significantly upregulated by 2.12-fold. The expression of *ykoV*, which belongs to the spore-encoded nonhomologous end-joining system, was upregulated by 1.58-fold in BS012. The expression of SOS regulator transcriptional repressor (*lexA*) was significantly downregulated. These results demonstrated that antioxidant compounds SqhC, SspA, and YkoV, sporulation-specific

genes, played important roles in resisting the oxidative stress of $VK_3$ in BS012.

## Discussion

Product toxicity plays a crucial role in assessing the feasibility of industrial microbial production. MK-7, a redox-active small molecule, can induce oxidative stress at high concentrations, limiting MK-7 production. However, the genotype–phenotype mapping relationship for MK-7 tolerance in *B. subtilis* is unclear, and host cells' tolerance cannot be improved by gene-targeting engineering techniques.

We used the ALE method to obtain BS012 with a tolerance from 6 mg/L to 60 mg/L $VK_3$. In static culture, BS012 can form robust biofilms both on solid surfaces (colonies) and gas–liquid surfaces (pellicles). However, domesticated strains of *B. subtilis*, utilized in laboratory research, had lost their ability to form robust biofilms (She et al. 2020); By measuring the $NADH/NAD^+$ ratio, the intracellular redox state of BS012 was more reduced than that of BS011. Then, a reduced redox state was sensed by cells, causing an increase in matrix production (Okegbe et al. 2014). Here, the matrix-dependent colony wrinkling in BS012 is required to increase the surface-to-volume ratio, thereby allowing cells in the biofilm greater access to oxygen and maintaining redox homeostasis (Kolodkin-Gal et al. 2013). Moreover, BS012 created pro-survival conditions for bacterial aggregate to resist the oxidative stress of $VK_3$. Genome resequencing results showed that *epsC*, *epsB*, and *sinR*, related to biofilm formation, all had mutations in BS012. Apart from that, we have verified that biofilm formation in *B. subtilis* is beneficial to the synthesis of MK-7 by fermentation. Similarly to our results, Cui et al. (Cui et al. 2020) confirmed that biofilms have effects on MK-7 synthesis by knocking out the biofilm-forming genes *epsA*, *epsB*, and *epsC* in *B. subtilis*. Wu et al. (Wu et al. 2021) knocked out *sinR*, resulting in an increased biofilm phenotype and MK-7 concentration. The state and composition of the cell membrane provided a stably synthesis and storage platform for MK-7 (Cui et al. 2020; Mahdinia et al. 2019).

In shake culture, BS012 cells were almost two-fold longer than BS011 after ALE. Genome resequencing data suggested that *walK*, coordinating cell wall remodel and cell division, had a mutation. From the transcriptome data, we can speculate that cells inhibit cell division by suppressing cell wall peptidoglycan synthesis, leading to larger cell size and smaller specific surface area, which in turn reduces the contact area of $VK_3$. At the same time, the inhibition of peptidoglycan synthesis also activates the expression of the σ-factor, which regulates the two-component system and cell wall homeostasis. After ALE, evolved strain BS012 shuts down the envelope stress response due to stress relief, leading to a downregulation of ECF $\sigma^M$ and $\sigma^V$. Additionally, saturated fatty acid synthesis was enhanced to ensure cell membrane stability and functionality and decrease cell membrane fluidity. Altogether, BS012 adapted to changes in the external environment through morphological changes, providing essential insights into the toxicity of fat-soluble VK. Our results are similar to those of previous studies that demonstrated an almost two-fold increase in cell elongation following butanol stress in *B. subtilis* (Gao et al. 2020; Vinayavekhin et al. 2015). The toxicity from high concentrations of VK to chassis cells has been neglected in microbial fermentation production, which may be an important factor hindering the industrial production scale of $VK_2$.

In shake culture, the T-AOC of BS012 was higher than that of BS011; transcriptome data suggested that bacteria reduce intracellular iron concentrations by limiting iron metabolism and the switch from aerobic to anaerobic nitrate respiration, consequently reducing ROS production (Anand et al. 2019; Zuber 2009). Furthermore, an antioxidant molecule (LMW thiol cysteine) plays an important role in resisting oxidative stress under high concentrations of $VK_3$; however, the reduction of the antioxidant molecule requires the consumption of intracellular reducing power NADPH, which also leads to the excessive consumption of carbon sources and the early activation of spore genes. Another reason for the upregulated expression of spore genes in BS012 was that both small acid-soluble spore protein and squalene cyclase were activated to further defense against $VK_3$ toxicity (Nagler et al. 2014).

Certain limitations arise from our research methodology. On the one hand, the sporulation may also have an indirect effect on the production of MK-7, resulting in a 22.2% increase in MK-7 production in BS012 compared with BS011. Whereas under static cultivation, spore formation slowed, leading to an MK-7 production increase of 76.0%. So slow sporulation under static culture conditions is beneficial for MK-7 production (Mahdinia et al. 2017). On the other hand, the robust biofilm formation sharply reduces the frequency of competent cells, resulting in the inability to perform genetic manipulation in BS012 (She et al. 2020). Thus, unambiguous evidence for the mutations' effects on BS012 leading to tolerance to $VK_3$ could not be produced. Hence, we decided to integrate the genomics analysis with RNA sequencing-based transcriptomics analysis to identify the most likely underlying reason for improved tolerance of $VK_3$ in BS012. $VK_3$ is a strongly oxidizing compound, and it is too hard to obtain strains with significantly enhanced antioxidant enzyme defenses in the vegetative and stationary phases by ALE alone. In the future, mutation breeding will be combined with ALE to obtain MK-7-producing strains with robust enzymatic defense systems, reducing the use of carbon by the non-enzymatic defense system during redox.

However, we surprisingly found that the highly tolerant MK-7-producing strain BS012 obtained by ALE has great promise for application in the food industry and could be developed as a probiotic preparation for patients with MK-7 deficiency. The main advantages are as follows: first, *B. subtilis* BS012 has various cell forms (vegetative cells and spores), and the characteristics of producing spores enable it to survive and function well in the gastrointestinal tract. Second, the formation of robust biofilms helps bacteria survive the acidic environment of the gastrointestinal tract. Finally, the activation of the anaerobic nitrate respiratory chain in BS012 ensured its normal metabolic function in the anaerobic environment of the gut. Therefore, BS012 may more easily survive and colonize the human gut. Compared to the existing MK-7 dietary supplement in the pharmaceutical market, the probiotics of BS012 can be used to maintain intestinal flora homeostasis, in addition to preventing osteoporosis and reducing the risk of cardiovascular disease. In addition to the above functions, *B. subtilis* biofilms are widely used for the biological control of plant roots (Vlamakis et al. 2013) and as "living materials" for various purposes (Zhang et al. 2019). Therefore, the ALE method for promoting biofilm formation is also suitable for the above research fields.

In general, we used the ALE to obtain BS012 with improved tolerance and MK-7 synthesis efficiency. Transcriptome analysis also showed that BS012 protected against oxidative damage by regulating cell morphology, antioxidant molecule levels, iron ion concentration, and the transition from aerobic to anaerobic respiration. Additionally, sporulation genes were activated in advance to further protect against DNA damage. Our study confirmed that improving the tolerance of *B. subtilis* to VK was an effective measure for increasing MK-7 production and preliminarily established the genotype–phenotype mapping relationships of *B. subtilis* tolerance to VK, providing a theoretical basis for producing other $VK_2$ subtypes by microbial fermentation.

**Supplementary Information** The online version contains supplementary material available at https://doi.org/10.1007/s00253-023-12877-7.

**Author contribution** DXM: investigation, methodology, data curation, and writing. ZZM: conceptualization, formal analysis, data curation, supervision, and funding acquisition. ZGH: review, editing, supervision, and funding acquisition. WL: conceptualization and resources. WH: investigation and data curation. WP: review and editing, supervision, and funding acquisition. All authors have given approval to the final version of the manuscript.

**Funding** This work was sponsored by financial support from the National Natural Science Foundation of China (12375352), China National Key Research and Development Program (2019YFA0904300 and 2019YFA0904304), the Major Projects of Science and Technology of Anhui Province (202103a06020003), and the National Natural Science Foundation of China (32070088).

**Data availability** The transcriptomics project was deposited in NCBI under the BioProject (https://www.ncbi.nlm.nih.gov/bioproject) accession number PRJNA899829. The sequencing data of the initial and evolved strains, BS011 and BS012, respectively, were deposited in the NCBI Sequence Read Archive (SRA; https://www.ncbi.nlm.nih.gov/sra) under accession numbers of SRR22245523, SRR22245524, SRR22245525, SRR22245526, SRR22245527, and SRR22245528. Other data that support the findings of this study are available in this published article and its Supplementary Material.

## Declarations

**Ethical approval** The article does not contain any studies with human participants or animals where ethical approval was required.

**Competing interests** The authors declare no competing interests.

## References

Anand A, Chen K, Yang L, Sastry AV, Olson CA, Poudel S, Seif Y, Hefner Y, Phaneuf PV, Xu S, Szubin R, Feist AM, Palsson BO (2019) Adaptive evolution reveals a tradeoff between growth rate and oxidative stress during naphthoquinone-based aerobic respiration. Proc Natl Acad Sci USA 116(50):25287–25292

Arjes HA, Vo L, Dunn CM, Willis L, DeRosa CA, Fraser CL, Kearns DB, Huang KC (2020) Biosurfactant-mediated membrane depolarization maintains viability during oxygen depletion in *Bacillus subtilis*. Curr Biol 30(6):1011-1022 e6

Berenjian A, Mahanama R, Talbot A, Regtop H, Kavanagh J, Dehghani F (2014) Designing of an intensification process for biosynthesis and recovery of menaquinone-7. Appl Biochem Biotechnol 172(3):1347–1357

Bitoun JP, Liao S, Yao X, Ahn SJ, Isoda R, Nguyen AH, Brady LJ, Burne RA, Abranches J, Wen ZT (2012) BrpA is involved in regulation of cell envelope stress responses in *Streptococcus mutans*. Appl Environ Microbiol 78(8):2914–2922

Chen T, Xia H, Cui S, Lv X, Li X, Liu Y, Li J, Du G, Liu L (2020) Combinatorial methylerythritol phosphate pathway engineering and process optimization for increased menaquinone-7 synthesis in *Bacillus subtilis*. J Microbiol Biotechnol 30(5):762–769

Commichau FM, Forchhammer K, Stülke J (2006) Regulatory links between carbon and nitrogen metabolism. Curr Opin Microbiol 9(2):167–172

Cui S, Lv X, Wu Y, Li J, Du G, Ledesma-Amaro R, Liu L (2019) Engineering a bifunctional Phr60-Rap60-Spo0A quorum-sensing molecular switch for dynamic fine-tuning of menaquinone-7 synthesis in *Bacillus subtilis*. ACS Synth Biol 8(8):1826–1837

Cui S, Xia H, Chen T, Gu Y, Lv X, Liu Y, Li J, Du G, Liu L (2020) Cell membrane and electron transfer engineering for improved synthesis of menaquinone-7 in *Bacillus subtilis*. iScience 23(3): 100918

Daskalaki A, Perdikouli N, Aggeli D, Aggelis G (2019) Laboratory evolution strategies for improving lipid accumulation in *Yarrowia lipolytica*. Appl Microbiol Biotechnol 103(20):8585–8596

Ding X, Zheng Z, Zhao G, Wang L, Wang H, Yang Q, Zhang M, Li L, Wang P (2022) Bottom-up synthetic biology approach for improving the efficiency of menaquinone-7 synthesis in *Bacillus subtilis*. Microb Cell Fact 21(1):101

Dorau R, Chen J, Liu J, Ruhdal Jensen P, Solem C (2021) Adaptive laboratory evolution as a means to generate *Lactococcus lactis* strains with improved thermotolerance and ability to autolyze. Appl Environ Microbiol 87(21):e0103521

Fang X, Yang Q, Liu H, Wang P, Wang L, Zheng Z, Zhao G (2019) Effects of a combined processing technology involving ultrasound and surfactant on the metabolic synthesis of vitamin $K_2$ by *Flavobacterium* sp. M1–14. Chem Eng Process 135:227–235

Fritsch VN, Loi VV, Busche T, Sommer A, Tedin K, Nürnberg DJ, Kalinowski J, Bernhardt J, Fulde M, Antelmann H (2019) The MarR-Type repressor MhqR confers quinone and antimicrobial resistance in *Staphylococcus aureus*. Antioxidants Redox Signaling 31(16):1235–1252

Fulaz S, Vitale S, Quinn L, Casey E (2019) Nanoparticle-biofilm interactions: the role of the EPS matrix. Trends Microbiol 27(11):915–926

Gao Y, Zhang M, Guo X, Li W, Lu D (2020) The biological mechanisms of butanol tolerance and the application of solvent-tolerant bacteria for environmental protection. J Chem Technol Biotechnol 95(5):1290–1297

Härtig E, Jahn D (2012) Regulation of the anaerobic metabolism in *Bacillus subtilis*. Adv Microbiol Physiol 61:195–216

Hederstedt L (2021) Molecular biology of *Bacillus subtilis* cytochromes anno 2020. Biochemistry (mosc) 86(1):8–21

Helmann JD (2016) *Bacillus subtilis* extracytoplasmic function (ECF) sigma factors and defense of the cell envelope. Curr Opin Microbiol 30:122–132

Hobley L, Ostrowski A, Rao FV, Bromley KM, Porter M, Prescott AR, MacPhee CE, Aalten DMFv, Stanley-Wall NR (2015) BslA is a self-assembling bacterial hydrophobin that coats the *Bacillus subtilis* biofilm. Proc Natl Acad Sci USA 112(38):E5371–E5375

Imber M, Pietrzyk-Brzezinska AJ, Antelmann H (2019) Redox regulation by reversible protein S-thiolation in Gram-positive bacteria. Redox Biol 20:130–145

Kolodkin-Gal I, Elsholz AKW, Muth C, Girguis PR, Kolter R, Losick R (2013) Respiration control of multicellularity in *Bacillus subtilis* by a complex of the cytochrome chain with a membrane-embedded histidine kinase. Genes Dev 27(8):887–899

Liao C, Ayansola H, Ma Y, Ito K, Guo Y, Zhang B (2021) Advances in enhanced menaquinone-7 production from *Bacillus subtilis*. Front Bioeng Biotechnol 9:695526

Loi VV, Rossius M, Antelmann H (2015) Redox regulation by reversible protein S-thiolation in bacteria. Front Microbiol 6:187

Luche S, Eymard-Vernain E, Diemer H, Van Dorsselaer A, Rabilloud T, Lelong C (2016) Zinc oxide induces the stringent response and major reorientations in the central metabolism of *Bacillus subtilis*. J Proteomics 135:170–180

Mahdinia E, Demirci A, Berenjian A (2017) Production and application of menaquinone-7 (vitamin K2): a new perspective. World J Microbiol Biotechnol 33(1):2

Mahdinia E, Demirci A, Berenjian A (2019) Biofilm reactors as a promising method for vitamin K (menaquinone-7) production. Appl Microbiol Biotechnol 103(14):5583–5592

Manjasetty BA, Chance MR, Burley SK, Panjikar S, Almo SC (2014) Crystal structure of *Clostridium acetobutylicum* aspartate kinase (CaAK): an important allosteric enzyme for amino acids production. Biotechnol Rep (amst) 3:73–85

Mavrommati M, Papanikolaou S, Aggelis G (2023) Improving ethanol tolerance of *Saccharomyces cerevisiae* through adaptive laboratory evolution using high ethanol concentrations as a selective pressure. Process Biochem 124:280–289

Mavrommati M, Daskalaki A, Papanikolaou S, Aggelis G (2021) Adaptive laboratory evolution principles and applications in industrial biotechnology. Biotechnol Adv:107795

Nagler K, Setlow P, Li Y, Ralf M (2014) High salinity alters the germination behavior of *Bacillus subtilis* spores with nutrient and nonnutrient germinants. Appl Environ Microbiol 80(4):8

Nakano MM, Zuber P (1998) Anaerobic growth of a "strict aerobe" (*Bacillus subtilis*). Annu Rev Microbiol 52:165–190

Okegbe C, Price-Whelan A, Dietrich LEP (2014) Redox-driven regulation of microbial community morphogenesis. Curr Opin Microbiol 18:39–45

Park SA, Bhatia SK, Park HA, Kim SY, Sudheer P, Yang YH, Choi KY (2021) *Bacillus subtilis* as a robust host for biochemical production utilizing biomass. Crit Rev Biotechnol 41(6):827–848

Pinochet-Barros A, Helmann JD (2018) Redox sensing by $Fe^{2+}$ in bacterial Fur family metalloregulators. Antioxidants Redox Signaling 29(18):1858–1871

Rao SPS, Alonso S, Rand L, Dick T, Pethe K (2007) The protonmotive force is required for maintaining ATP homeostasis and viability of hypoxic, nonreplicating *Mycobacterium tuberculosis*. Proc Natl Acad Sci USA 105(33):11945–11950

Ren L, Peng C, Hu X, Han Y, Huang H (2020) Microbial production of vitamin $K_2$: current status and future prospects. Biotechnol Adv 39:107453

She Q, Hunter E, Qin Y, Nicolau S, Zalis EA, Wang H, Chen Y, Chai Y (2020) Negative interplay between biofilm formation and competence in the environmental strains of *Bacillus subtilis*. mSystems 5(5)

Shen J, Liu Z, Yu H, Ye J, Long Y, Zhou P, He B (2020) Systematic stress adaptation of *Bacillus subtilis* to tetracycline exposure. Ecotoxicol Environ Saf 188:109910

Su Y, Liu C, Fang H, Zhang D (2020) *Bacillus subtilis*: a universal cell factory for industry, agriculture, biomaterials and medicine. Microb Cell Fact 19(1):173

Sun X, Ren L, Bi Z, Ji X, Zhao Q, Huang H (2018a) Adaptive evolution of microalgae *Schizochytrium* sp. under high salinity stress to alleviate oxidative damage and improve lipid biosynthesis. Bioresour Technol 267:438–444

Sun X, Ren L, Zhao Q, Ji X, Huang H (2018b) Microalgae for the production of lipid and carotenoids: a review with focus on stress regulation and adaptation. Biotechnol Biofuels 11:272

van der Reest J, Lilla S, Zheng L, Zanivan S, Gottlieb E (2018) Proteome-wide analysis of cysteine oxidation reveals metabolic sensitivity to redox stress. Nat Commun 9(1):1581

Vinayavekhin N, Mahipant G, Vangnai AS, Sangvanich P (2015) Untargeted metabolomics analysis revealed changes in the composition of glycerolipids and phospholipids in *Bacillus subtilis* under 1-butanol stress. Appl Microbiol Biotechnol 99(14):5971–5983

Vlamakis H, Chai Y, Beauregard P, Losick R, Kolter R (2013) Sticking together: building a biofilm the *Bacillus subtilis* way. Nat Rev Microbiol 11(3):157–168

Wang H, Liu H, Wang L, Zhao G, Tang H, Sun X, Ni W, Yang Q, Wang P, Zheng Z (2019) Improvement of menaquinone-7 production by *Bacillus subtilis natto* in a novel residue-free medium by increasing the redox potential. Appl Microbiol Biotechnol 103(18):7519–7535

Wu J, Li W, Zhao SG, Qian SH, Wang Z, Zhou MJ, Hu WS, Wang J, Hu LX, Liu Y, Xue ZL (2021) Site-directed mutagenesis of the quorum-sensing transcriptional regulator SinR affects the biosynthesis of menaquinone in *Bacillus subtilis*. Microb Cell Fact 20(1):113

Yang S, Cao Y, Sun L, Li C, Lin X, Cai Z, Zhang G, Song H (2019) Modular pathway engineering of *Bacillus subtilis* to promote de novo biosynthesis of menaquinone-7. ACS Synth Biol 8(1):70–81

Zhang C, Huang J, Zhang J, Liu S, Cui M, An B, Wang X, Pu J, Zhao T, Fan C, Lu TK, Zhong C (2019) Engineered *Bacillus subtilis* biofilms as living glues. Mater Today 28:40–48

Zuber P (2009) Management of oxidative stress in *Bacillus*. Annu Rev Microbiol 63:575–597